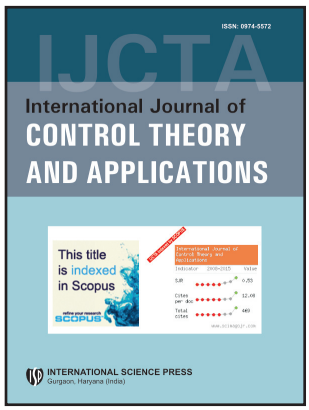

International Journal of Control Theory and Applications

ISSN : 0974-5572

Volume 10 • Number 25 • 2017

Identification of Vegetation by using Particle Swarm Optimization

Rincy Merlin Mathew[a], S. Purushothaman[b] and P. Rajeswari[c]

[a]*Research Scholar, Department of MCA, VELS University, Pallavaram, Chennai, India-600117*
[b]*Chennai. Email: dr.s.purushothaman.2015@gmail.com*
[c]*Department of Computer Science Girls Community College, King Khalid University, Abha, Saudi Arabia. Email: dr.p.rajeswari@gmail.com*

Abstract: An implementation of particle swarm optimization (PSO) for segmentation of multispectral Landsat vegetation image is presented. The required band Landsat 8 (5, 4, 3) and Landsat 7 (4, 3, 2) are considered from the multispectral image for segmentation and identification of vegetation. Two sample images: one from ERDAS format acquired by Landsat 7 'Paris.lan' (band 4, band 3, Band 2) and another image acquired from Landsat 8 (band 5, band 4, band 3) are used in this paper. PSO is used to segment the plane-1(Near infra red spectra) and plane 2(RED spectra). The monochrome of the two segmented images is compared with a monochrome of the images without PSO segmentation.

Keywords: Multispectral image; vegetation identification; particle swarm optimization (PSO);

1. INTRODUCTION

Remote sensing is a process of collecting information on the earth's surface by using satellites from different heights above the earth's surface. Digital cameras that capture multispectral wavelengths are fixed to the satellites. The satellites move along latitude and longitude to cover a specific area repeatedly. The number of times the satellite visit a specific area per day depends on the speed of the satellite.

2. RELATED WORK

Masroor et. al., 2013, discussed the traditionally pixel-based and statistics-oriented change detection techniques which focus mainly on the spectral values and ignore the spatial context. A review of object-based change detection techniques is compassed. Also, a study on the spatial data mining techniques in image processing and change detection from remote sensing data is discussed. The significance of the rapid change in the image data volume and multiple sensors and related confrontations on the growth of change detection techniques are highlighted.

Hannes et. al., 2016, introduced the importance of annual deforestation information for understanding and alleviating deforestation. An image compositing approach is used to transform 2224 Landsat images in a spatially

continuous and cloud free environment. Also, a random forest classifier is used to derive annual deforestation patterns.

Pasher et. al., 2016, introduced methods for earth observation that can be used to enumerate and keeps track of linear woody features across the environment. In the meanwhile, individual structure can be manually systemized and is concentrated on the enhancement of methods using line intersect sampling for estimating linear woody features as an indicator of environmental assessment in agricultural topography. Curtis et. al., 2016, evaluated the significance of topographic correction on trend-based forest change detection conclusions by analyzing the location and an aggregation of changes is classified on an image synthesis with and without a topographic correction. A large amount of change in area is identified when No. topographic rectification is correlated to the synthesized image.

Zhao-Liang et. al., 2013, reviewed the present significance of certain remote sensing algorithms for estimating LST from thermal infrared (TIR) data. A survey on algorithms to gain LST from space-based TIR measurements is accomplished based on the speculated circumstances. Also, an emphasis on TIR data obtained from polar-orbiting satellites is done due to the extensive use, comprehensive relevance and higher spatial resolution in contradiction to geostationary satellites.

O'Loughlin et. al., 2016, developed the first global 'Bare-Earth' Digital Elevation Model based on the Shuttle Radar Topography Mission for all landmasses between 60N and 54S..

Andrew et. al., 2016, introduced methods by using a small, unpiloted aerial system to acquire aerial photographs and processing these using structure-from-motion photogrammetry, three-dimensional models were generated. The models describe the vegetation.

Min Feng et. al., 2016, estimated a mechanism based on per-pixel estimates of percentage tree cover and their associated uncertainty, the dataset currently signifies binary forest cover in nominal 1990, 2000, and 2005 epochs, besides gains and losses due to time.

Mihretab et. al., 2016, introduced methods for the supervised classification technique to classify and analyze the total forest-cover change in Eritrea.

Mohamed et. al., 2016 developed a GIS for comparing the appropriate method for main crops based on the needs of the crops and the quality and properties of land.

Yu Zhang et. al., 2016, analyzed a study on the configurations and spatial-temporal processes of landscape. The results of the variation partitioning of the landscape indicated complex interrelationships among all of the pairs of driver sets.

Adrien Michez et. al., 2016, proposed a technique for an easily reproducible approaches framework using Unmanned Aerial Systems (UAS) imagery.

Gayantha et. al., 2016, developed extraction of spectrally pure pixels of a given area. using Pixel Purity Index (PPI), identification of the selected end member spectrum using the Modified Gaussian Method(MGM) and mapping of logically identified end members using the Spectral Angle Mapper (SAM) method. Mapping results determine both the capabilities and the limitations of the MGM method of convolution and the SAM method of spectral matching as efficient tools for compositional representation of morphological appearance on the lunar surface.

Inka et. al., 2016, examined the classification of forest land using airborne laser scanning data.

Trung et. al., 2016, used Spatial-Temporal Adaptive Algorithm for mapping Reflectance Change. Robinson et. al., 2016, tested the capability of WV2 imagery. New generation satellite sensors are removing

barriers from previously preventing widespread adoption of remote sensing technologies in natural resource management.

3. METHODOLOGY

Data Collection: Multispectral Landsat images are used in this paper.

Sample-1 Image: The image taken from Landsat 7 with ERDAS format is presented. It has seven bands. Band 4, 3, 2 are considered for segmentation.

Figure 1: Multispectral composite image (Band 4, 3, 2)

Courtesy: Space Imaging and Math Works: Figure 1 shows an RGB image with false colours. Figure 2 shows an enhanced image of the RGB with an increase in the intensity values.

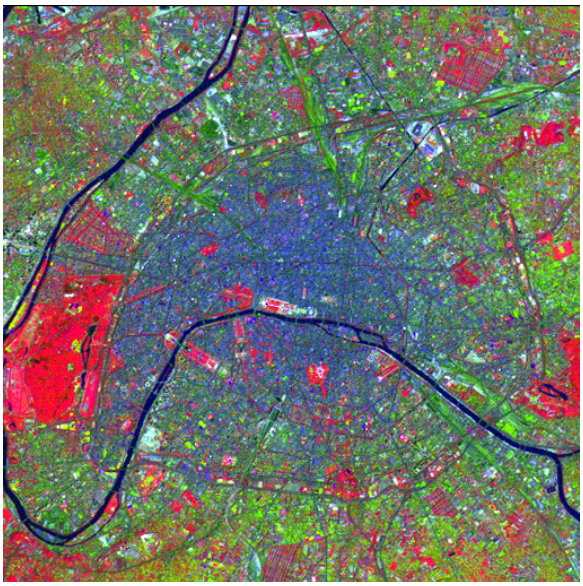

Figure 2: Enhanced image with decorrelation function in Matlab

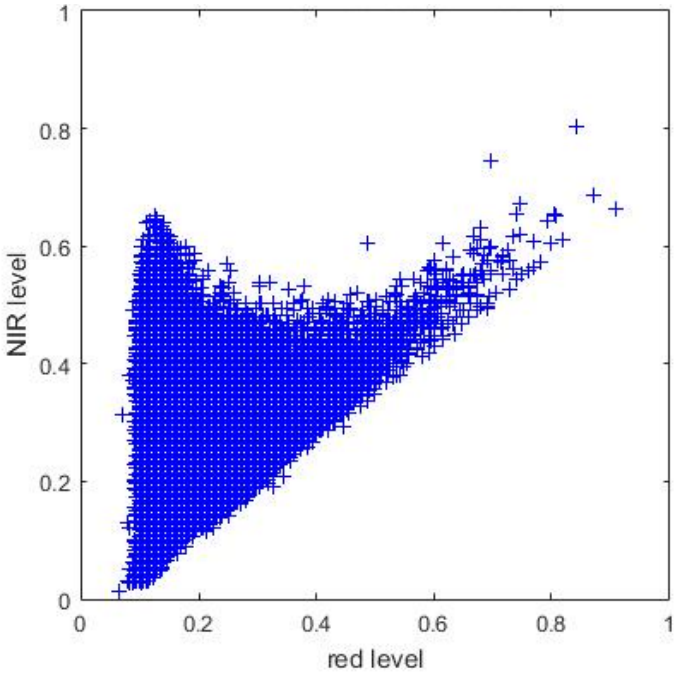

Figure 3: Scatter plot

Figure 3 presents a scatter plot with RED spectra versus NIR spectra values from the RG planes of Figure 2.

Normalized Difference Vegetation Index(NDVI): It is the most commonly used Vegetation Index, as it enables to eliminate topographic effects and variations in the sun illumination angle, as well as other atmospheric elements such as haze. NDVI images, in contrast to RATIO, have normal distribution given by equation (1).

$$\text{NDVI} = \frac{\text{NIR} - \text{R}}{\text{NIR} + \text{R}} \tag{1}$$

Figure 4 presents the normalized difference vegetation index.

Figure 5 presents an image with threshold = 0.4 applied.

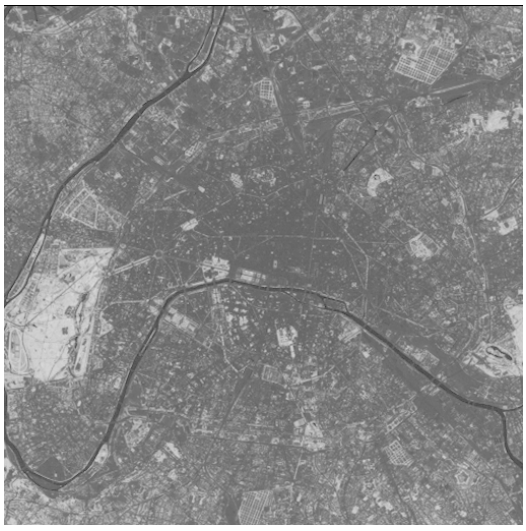

Figure 4: NDVI with gray scale

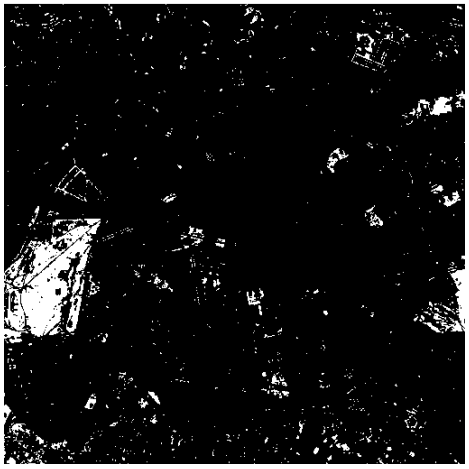

Figure 5: NDVI with threshold = 0.4 applied

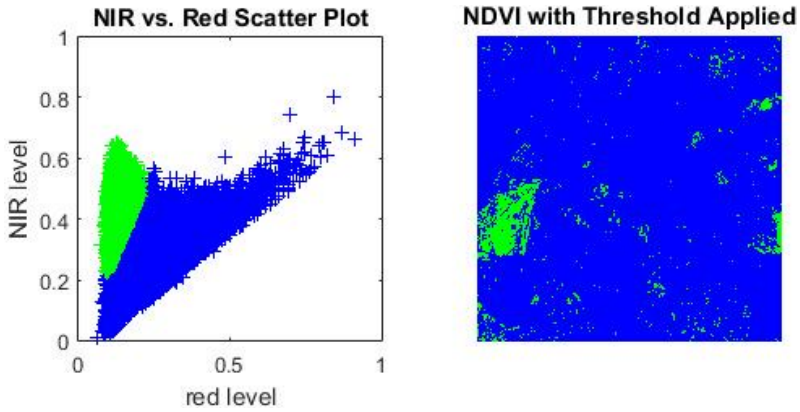

(a) **(b)**

Figure 6: (a) Scatter plot with vegetation and (b) Presence of vegetation (green color)

Figure 6(a) shows the ration of green vegetation with other information (blue). Figure 6(b) presents the distribution of vegetation (green) in the original image (Figure 2)

Sample-2 Image: Figure 7 presents Landsat 8 "R G B = 4 3 2" image showing vegetation.

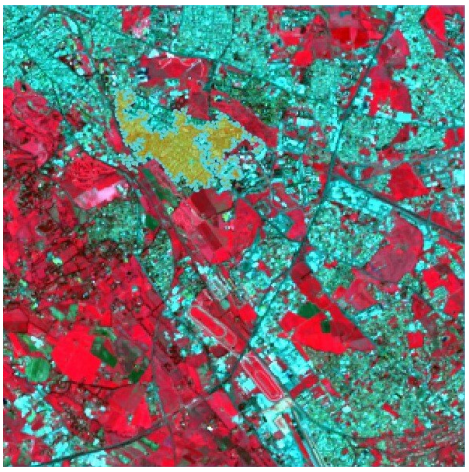

Figure 7: Landsat-8 composite image

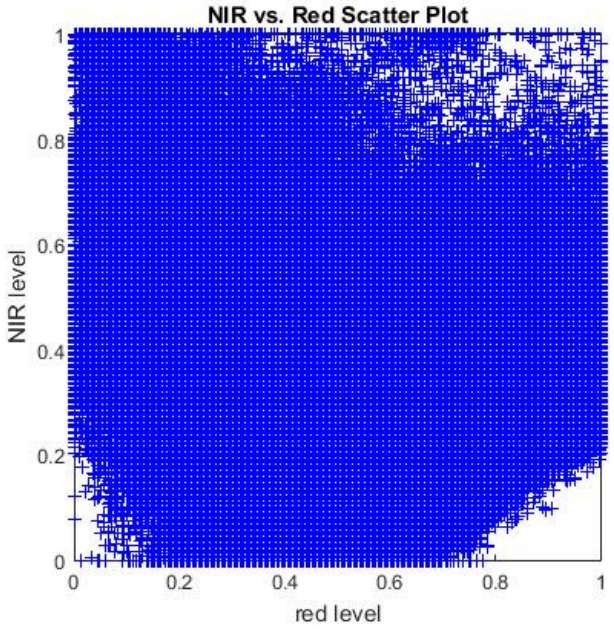

Figure 8: Scatter plot

Figure 8 presents a scatter plot of RED spectra versus NIR spectra values from the RG planes of Figure 7.

Figure 9 presents the normalized difference vegetation index.

Figure 10 presents an image with threshold = 0.4 applied.

Figure 11(a) shows the ration of green vegetation with other information (blue). Figure 11(b) presents the distribution of vegetation (green) in the original image (Figure 7).

Particle swarm optimization: What birds searching for food is described by the particle swarm optimization algorithm. They try to locate food at far away distance. A bird is called particle. A desired target or association value is evaluated by using a target objective function. This helps if the birds have reached their food. The birds move with specific velocities and directions to reach the food.

The concept of generations is used for searching the location of food. Two best values are used in each generation. Present best value and global best value.

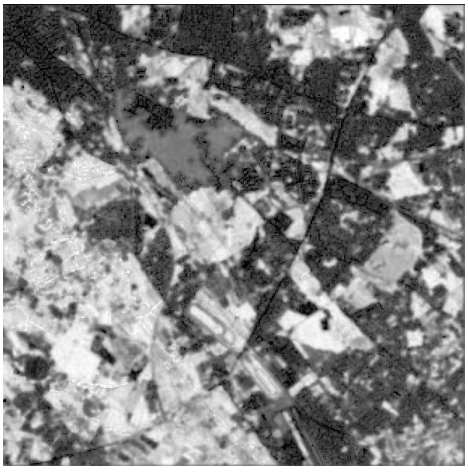

Figure 9: NDVI with gray scale

Figure 10: NDVI with threshold=0.4 applied

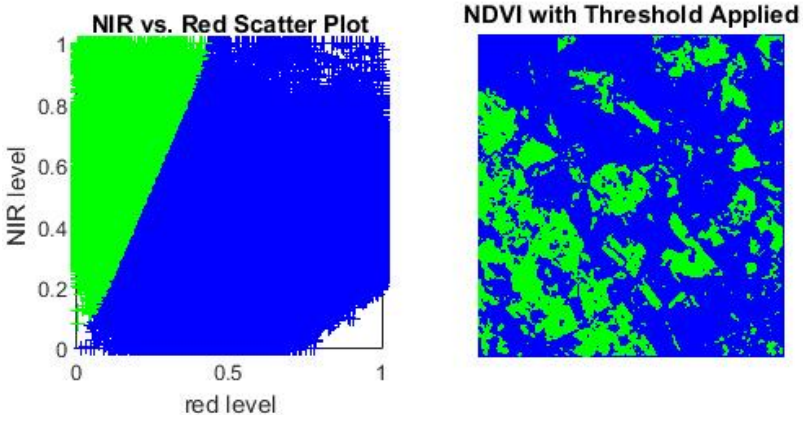

(a) **(b)**

Figure 11: (a) Scatter plot with vegetation and (b) Presence of vegetation (green color)

By using the calculated values, the velocity of the particles and their positions are updated by (2) and (3).

$$\text{vel}[] = \text{vel}[] + Fc1 \times \text{randnumber} \times (\text{presentbest}[] - \text{current values}[]) + Fc2 \times \text{randnumber} \times (\text{globalbest}[] - \text{currentvalue}[]) \quad (2)$$

$$\text{currentvalue}[] = \text{currentvalue}[] + \text{vel}[] \quad (3)$$

vel[] represents the velocity of the particles,

currentvalue[] is the current particle position.

Fc1, Fc2 are learning factors.

PSO Parameter Control

Based on the population of particles: It can be anything of our choice according to the problem. It can be up to 1000 as well.

Based on the maximum velocity: It indicates velocity changes. Maximum velocity can be any value split into a range from negative to positive.

Based on the knowledge of learning: Fc1 and Fc2 usually can be any value greater than 0.

Based on the program termination: The maximum number of iterations the PSO execute and the minimum error requirement.

Sample-1 Image: PSO segmentation of NIR and Red spectral bands

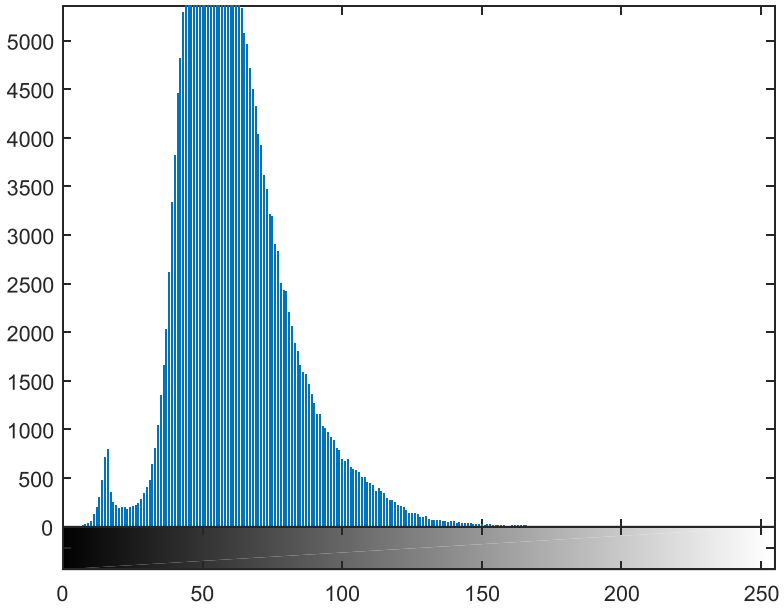

Figure 12: Histogram of NIR Band-4

Figure 12 presents the histogram of the NIR image. Figure 15 presents a histogram of the RED image. The plots show an inclination towards left-hand side and hence more toward black. The plots show it is not normally distributed.

Figure 13 shows NIR PSO segmented in the grey scale image and Figure 14 shows NIR PSO segmented in a monochrome image.

Figure 16 shows RED PSO segmented in the grey scale image and Figure 17 shows RED PSO segmented in a monochrome image.

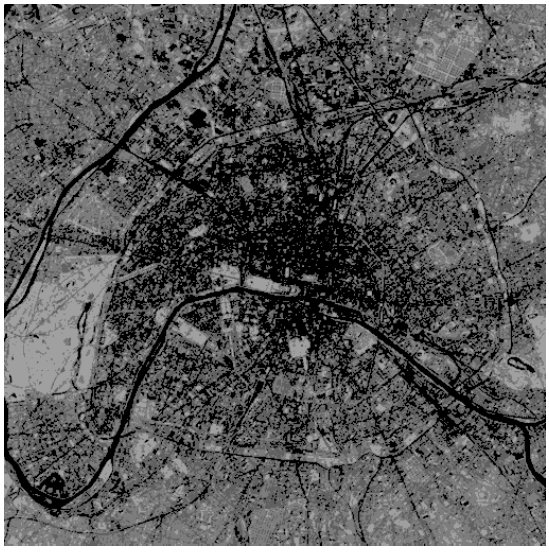

Figure 13: PSO Segmented NIR in gray scale image

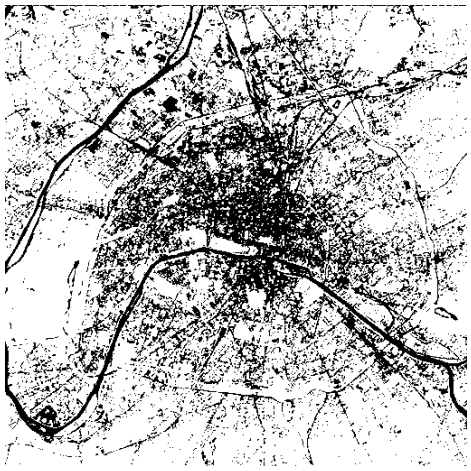

Figure 14: PSO Segmented NIR in monochrome image

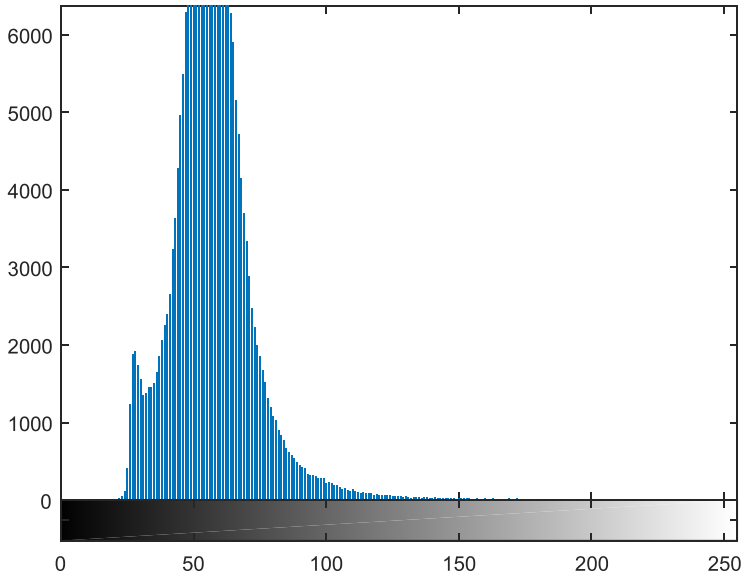

Figure 15: Histogram of RED band-3

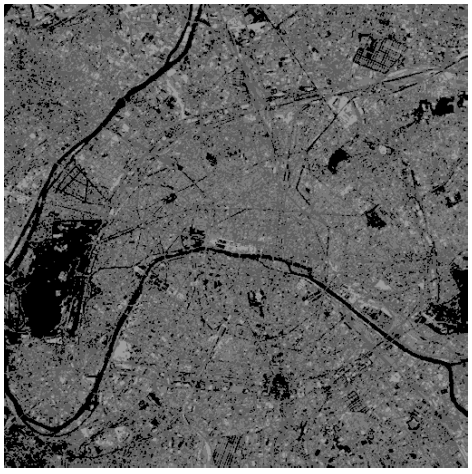

Figure 16: PSO Segmented RED in gray scale image

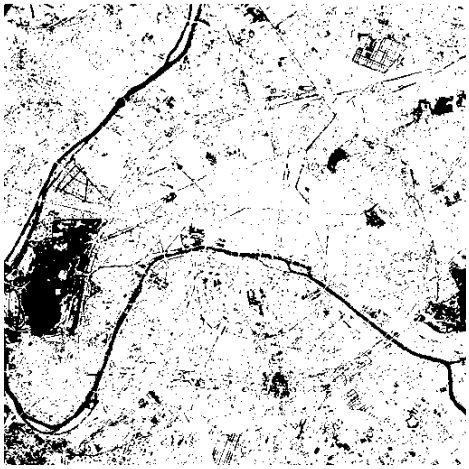

Figure 17: PSO Segmented RED in monochrome image

Sample-2 Image: Figure 18 presents histogram for the NIR image. The histogram is normally distributed. Figure 21 presents histogram for the RED image. The histogram is normally distributed.

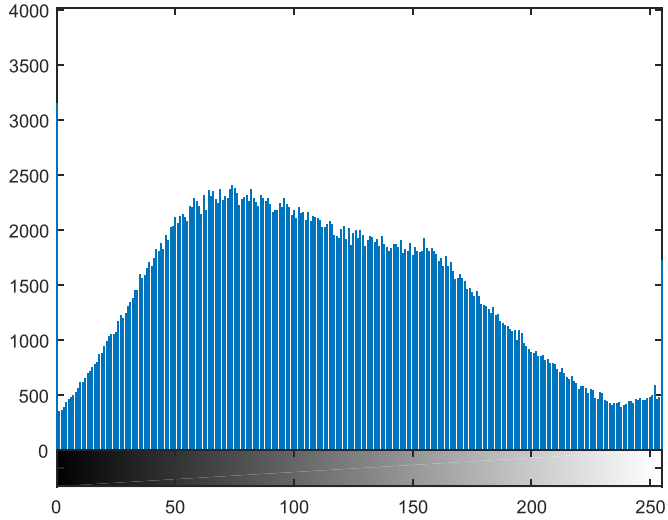

Figure 18: Histogram of NIR band-5

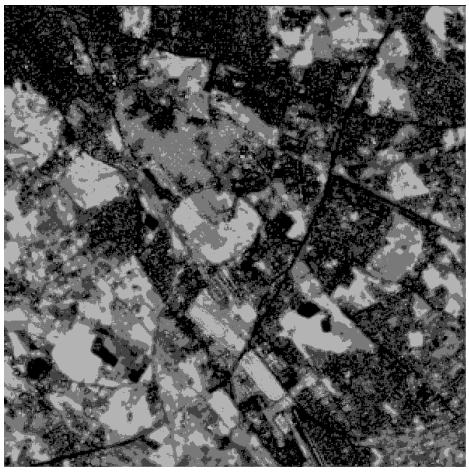

Figure 19: PSO Segmented NIR in gray scale

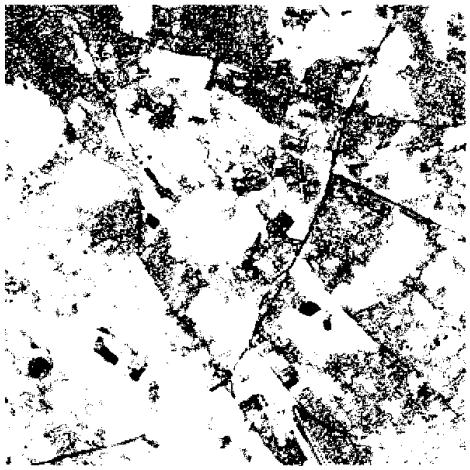

Figure 20: PSO Segmented NIR in monochrome image

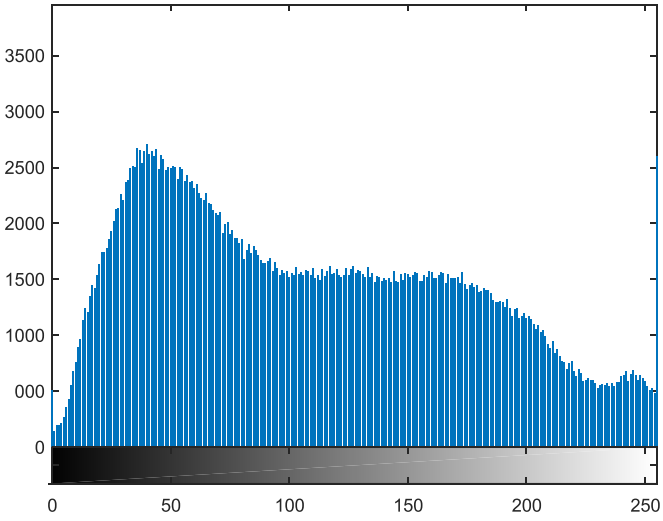

Figure 21: Histogram of RED band-4

Figure 19 presents the PSO segmented NIR image in gray scale, and Figure 20 presents PSO segmented monochrome of the NIR image.

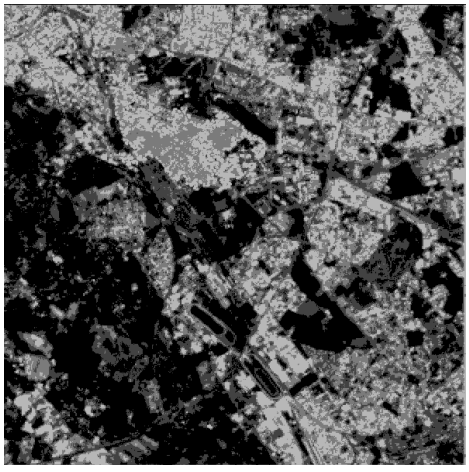

Figure 22: PSO Segmented RED band in gray scale

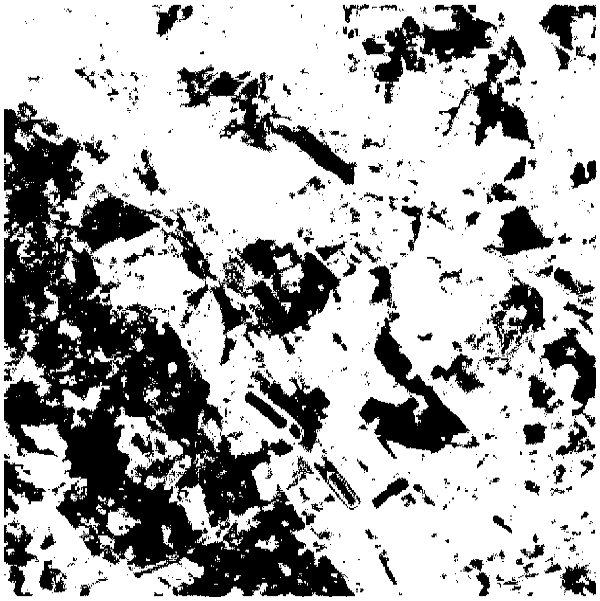

Figure 23: Segmented RED band in monochrome image

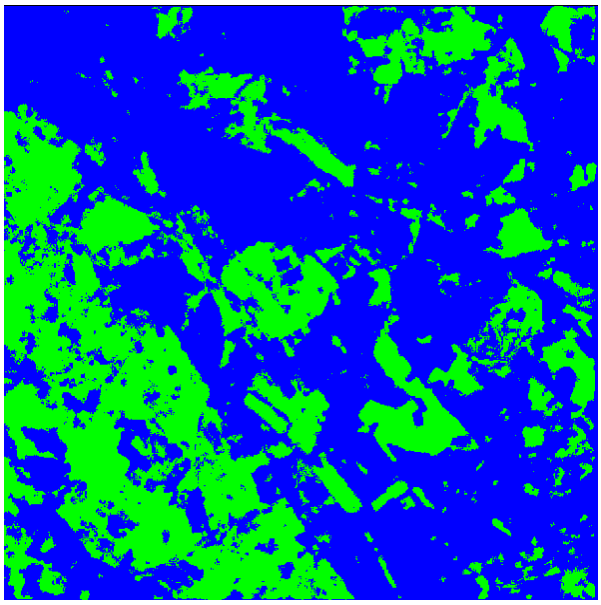

Figure 24: Presence of vegetation (green color)

Figure 22 presents the PSO segmented RED band in gray scale, and Figure 23 presents PSO segmented monochrome of the RED band. Figure 24 presents the distribution of vegetation (green) in the original image (Figure 7).

4. RESULTS AND DISCUSSIONS

Training the Particle swarm optimization

Figure 25 presents initial particles positions and Figure 26 presents the movement of particles in two iterations. Figure 27 shows the plot of a function and the path in which the particles moved. This plot shows for two iterations.

Figure 25: Particles in the initial matrix

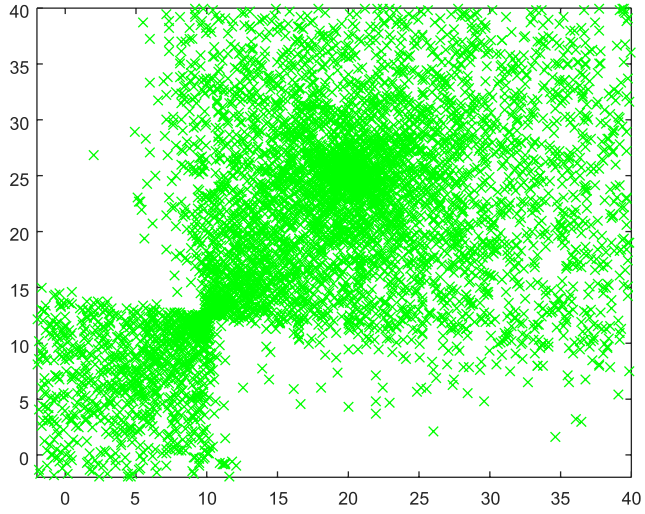

Figure 26: Particles after two iterations

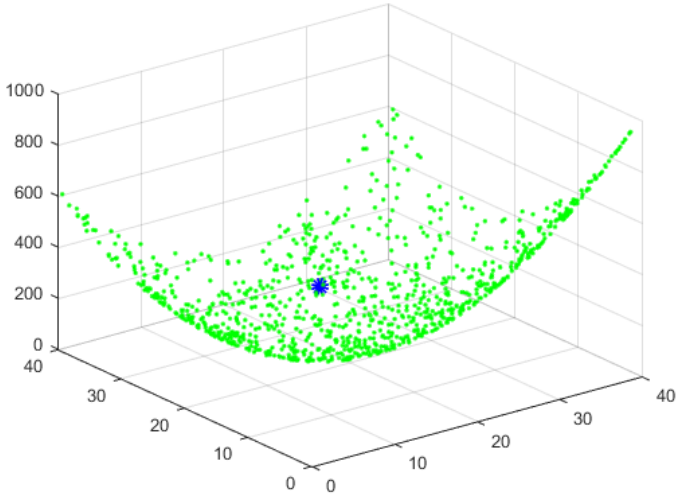

Figure 27: Fitness plot

Training parameters

N = 150; population size

N_PAR = level-1; Number of thresholds

Iterations = 150; number of iterations

PHI1 = 0.8; individual weight of particles

PHI2 = 0.8; other weight of particles

W = 1.2; inertial factor

vmin = −5;

vmax = 5;

globalbestvalueR = −10000;

Find the probability of each intensity values

Receiver Operating Characteristic Curve

ROC curve provides the performance of the algorithms in classification, especially in pattern recognition. Each point in the curve is plotted with false positive rate (FPR) in *x*-axis versus true positive rate (TPR) in the *y*-axis. A point in the curve is obtained by considering a minimum of 10 pairs of cover and message images. ROC curve (Figure 9) is drawn using a set of positive and negative outputs.

(i) **True positive (TP):** If the image contains vegetation information, and if the algorithm identifies it correctly, then it is truly positive.

(ii) **False negative (FN):** If the image contains vegetation information, and if the algorithm says No. vegetation, then it is false negative.

(iii) **True negative (TN):** If the image does not contain vegetation information, and if the algorithm does not identify it, then it is truly negative.

(iv) **False positive (FP):** If the image does not contain vegetation informaiton, and if the algorithm says there is vegetation information, then it is false positive.

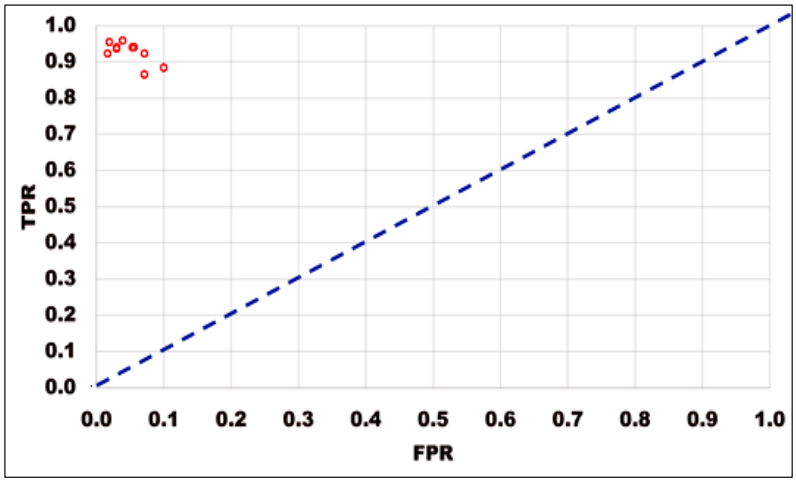

Figure 28: ROC for recovery algorithm

$$\text{True positive rate (TPR)} = \frac{TP}{TP + FN} \tag{3}$$

$$\text{False positive rate (FPR)} = \frac{FP}{FP + TN} \tag{4}$$

Figure 28 presents ROC for the performance of PSO algorithm. The points plotted are above diagonal in the ROC plot which is acceptable. The diagonal is drawn from left bottom to the right top of the plot (blue dots). Hence, PSO performance in segmentation of the multispectral image is good.

5. CONCLUSIONS

Particle swarm optimization algorithm has been implemented in Matlab 2015 for segmentation of Landsat 7 and Landsat 8 images that show land cover vegetation. The segmentation of the PSO is compared with the method of identifying vegetation without PSO segmentation.

REFERENCES

[1] Masroor Hussain, Dongmei Chen, Angela Cheng, Hui Wei, and David Stanley, (2013), Change detection from remotely sensed images: From pixel-based to object-based approaches, ISPRS Journal of Photogrammetry and Remote Sensing, Vol. 80, pp. 91–106.

[2] Hannes Müller, Patrick Griffiths, and Patrick Hostert, (2016), Long-term deforestation dynamics in the Brazilian Amazon—Uncovering historic frontier development along the Cuiabá–Santarém highway, International Journal of Applied Earth Observation and Geoinformation, Vol. 44, pp. 61–69.

[3] Pasher J., McGovern M., and Putinski V., (2016), Measuring and monitoring linear woody features in agricultural landscapes through earth observation data as an indicator of habitat availability, International Journal of Applied Earth Observation and Geoinformation, Vol. 44, pp.113–123.

[4] Curtis M. Chance, Txomin Hermosilla, Nicholas C. Coops, Michael A. Wulder, and Joanne C. White, (2016), Effect of topographic correction on forest change detection using spectral trend analysis of Landsat pixel-based composites, International Journal of Applied Earth Observation and Geoinformation, Vol. 44, pp.186–194.

[5] Zhao-Liang Li, Bo-Hui Tang, Hua Wu, Huazhong Ren, Guangjian Yan, Zhengming Wan, Isabel F. Trigo, and José A. Sobrino, (2013), Satellite-derived land surface temperature: Current status and perspectives, Remote Sensing of Environment, Vol. 131, pp. 14–37.

[6] O'Loughlin F.E, Paiva R.C.D, Durand M., Alsdorf D.E, and Bates P.D., (2016), A multi-sensor approach towards a global vegetation corrected SRTM DEM product, Remote Sensing of Environment, Vol. 182, pp. 49–59.

[7] Andrew M. Cunliffe, Richard E. Brazier, and Karen Anderson, (2016), Ultra-fine grain landscape-scale quantification of dryland vegetation structure with drone-acquired structure-from-motion photogrammetry, Remote Sensing of Environment, Vol. 183, pp. 129–143.

[8] Min Feng, Joseph O. Sexton, Chengquan Huang, Anupam Anand, Saurabh Channan, Xiao-Peng Song, Dan-Xia Song, Do-Hyung Kim, Praveen Noojipady, and John R. Townshend, (2016), Earth science data records of global forest cover and change: Assessment of accuracy in 1990, 2000, and 2005 epochs, Remote Sensing of Environment, Vol. 184, pp. 73–85.

[9] Mihretab G. Ghebrezgabher, Taibao Yang, Xuemei Yang, Xin Wang, and Masihulla Khan, (2016), Extracting and analyzing forest and woodland cover change in Eritrea based on landsat data using supervised classification, The Egyptian Journal of Remote Sensing and Space Sciences, Vol. 19, pp. 37–47.

[10] Mohamed A.E. AbdelRahman, A. Natarajan, and Rajendra Hegde, (2016), Assessment of land suitability and capability by integrating remote sensing and GIS for agriculture in Chamarajanagar district, Karnataka, India, The Egyptian Journal of Remote Sensing and Space Sciences, Vol. 19, pp.125–141.

[11] Yu Zhang, Tianwei Wang, Chongfa Cai, Chongguang Li, Yaojun Liu, Yuze Bao, and Wuhong Guan, (2016), Landscape pattern and transition under natural and anthropogenic disturbance in an arid region of north western China, International Journal of Applied Earth Observation and Geoinformation, Vol. 44, pp.1–10.

[12] Adrien Michez, Hervé Piégay, Lisein Jonathan, Hugues Claessens, and Philippe Lejeune, (2016), Mapping of riparian invasive species with supervised classification of Unmanned Aerial System (UAS) imagery, International Journal of Applied Earth Observation and Geoinformation, Vol. 44, pp. 88–94.

[13] Gayantha R.L. Kodikara, Champati ray P.K., Prakash Chauhan, and Chatterjee R.S., (2016), Spectral mapping of morphological features on the moon with MGM and SAM, International Journal of Applied Earth Observation and Geoinformation, Vol. 44, pp. 31–41.

[14] Inka Pippuri, Aki Suvanto, Matti Maltamo, Kari T. Korhonen, Juho Pitkänen, and Petteri Packalen, (2016), Classification of forest land attributes using multi-source remotely sensed data, International Journal of Applied Earth Observation and Geoinformation, Vol. 44, pp. 11–22.

[15] Trung V. Tran, Kirsten M. de Beurs, and Jason P. Julian, (2016), Monitoring forest disturbances in Southeast Oklahoma using Landsatand MODIS images, International Journal of Applied Earth Observation and Geoinformation, Vol. 44, pp.42–52.

[16] Robinson T.P., Wardell-Johnson G.W., Pracilio G., Brown C., Corner. R, and van Klinken R.D., (2016), Testing the discrimination and detection limits of WorldView-2imagery on a challenging invasive plant target, International Journal of Applied Earth Observation and Geoinformation, Vol. 44, pp. 23–30.